

## A Small Satellite Payload for Airglow Measurements in the Upper Atmosphere by Spatial Heterodyne Interferometry

Friedhelm Olschewski

University of Wuppertal, Institute for Atmospheric and Environmental Research  
Gauss-Strasse 20, 42119 Wuppertal, Germany; (+49) 202-439-2929  
olsch@uni-wuppertal.de

Martin Kaufmann

Research Center Juelich, Institute of Energy and Climate Research Stratosphere (IEK-7)  
Wilhelm-Johnen-Strasse, 52428 Juelich, Germany; (+49) 2461-61-5250  
m.kaufmann@fz-juelich.de

Klaus Mantel

Max Planck Institute for the Science of Light  
Staudtstrasse 2, 91058 Erlangen, Germany, Germany; (+49) 9131-7133732  
klaus.mantel@mpl.mpg.de

Tom Neubert, Heinz Rongen

Research Center Juelich, Central Institute of Engineering, Electronic Systems (ZEA-2)  
Wilhelm-Johnen-Strasse, 52428 Juelich, Germany; (+49) 2461-61-4512  
First Author's Email

Martin Riese

Research Center Juelich, Institute of Energy and Climate Research Stratosphere (IEK-7)  
Wilhelm-Johnen-Strasse, 52428 Juelich, Germany; (+49) 2461-61-2065  
m.riese@fz-juelich.de

Ralf Koppmann

University of Wuppertal, Institute for Atmospheric and Environmental Research  
Gauss-Strasse 20, 42119 Wuppertal, Germany; (+49) 202-439-2605  
koppmann@uni-wuppertal.de

### ABSTRACT

A novel small satellite payload for atmospheric research has been developed to study the temperature distribution in the mesosphere and lower thermosphere region. The payload consists of a small interferometer for the observation of airglow at 762 nm. The line intensities of the O<sub>2</sub> A-band emissions are used to derive temperatures in the upper atmosphere. The temperature data will be used to analyze dynamical wave structures in the atmosphere which are important for modeling of the climate system.

Integrated in a small satellite or a 6U CubeSat, the instrument needs a highly accurate attitude determination and control systems in the sub-arcmin range for limb sounding of the atmosphere. The payload electronics concept is based on a System-on-Module architecture which combines reconfigurable hardware with a processing unit as a highly integrated component. The agility of a CubeSat or the maneuverability of a small satellite can be used to focus the measurements on specific regions in the atmosphere from different viewing directions. Three-dimensional images of an atmospheric volume can be derived using tomographic reconstruction techniques.

A prototype of this payload, launched on a Chinese technology demonstration satellite in December 2018, proved the practical usability of this instrument design.

## INTRODUCTION

Dynamical processes in the mesosphere and lower thermosphere (MLT) region are still an important research topic. The region where space weather meets Earth's atmosphere and vice versa, plays an important role in climate modelling. Studying processes in the upper atmosphere will help to improve the understanding of potential anthropogenic effects on the climate system<sup>1,2</sup>. Unresolved small scale processes like gravity waves lead to large uncertainties in climate modelling<sup>3</sup>. The impact of gravity-wave drag on large-scale dynamics requires global measurements at high spatial resolution.

As the MLT region is dominated by waves which influence the wind and temperature fields of this altitude range, coupling processes initiated by gravity waves in the middle atmosphere have increasing importance for the modeling of the climate system and represent one of the larger uncertainties in this field, because gravity waves are one of the least explored dynamical processes in the middle and upper atmosphere. They are mostly generated in the troposphere, propagate vertically and horizontally, carrying momentum from the troposphere up to the stratosphere, mesosphere and even to the thermosphere. The wavelength range of these waves is in the order of several kilometers in the vertical and from tens to hundreds of kilometers in the horizontal. When gravity waves break, they deposit their momentum at that particular region of the atmosphere. This phenomenon is the key driver for the summer-to-winter pole circulation at the mesopause and one of the most uncertain parameters in climate models.

In a study using the NCAR Whole Atmosphere Community Climate Model (WACCM) the dynamical influence of the lower and middle atmosphere on the upper mesosphere and lower thermosphere was investigated<sup>4</sup>. The results show a strong dependency on the method used for representing gravity wave drag. This demonstrates the role of gravity waves in transporting the variability of the troposphere into the mesosphere and lower thermosphere. The diversity of gravity wave generation and breaking in the atmosphere is described by Kim et al., 2003<sup>5</sup>.

## DYNAMICAL STRUCTURES DETECTED IN MLT TEMPERATURE DISTRIBUTION

Gravity waves affect the temperature fields of the atmosphere and can be detected by measuring the temperature distribution in the region of interest<sup>7</sup>. Figure 1 demonstrates the influence of a gravity wave on the temperature distribution between 86 km and 104 km in a simulation run. The horizontal axis in the figure

covers several hundred kilometers with several wave cycles clearly visible. The amplitude of the temperature variation rises up to +/- 5 K.

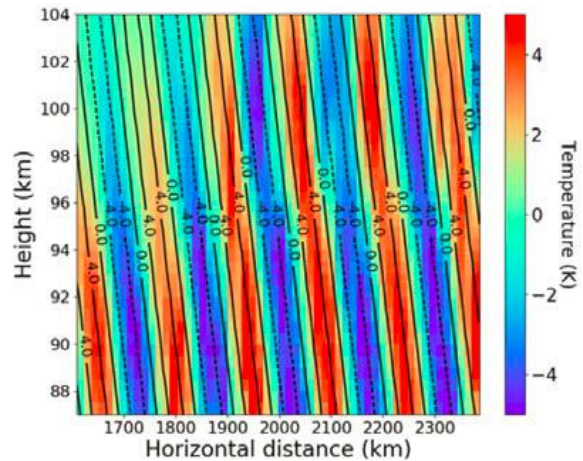


**Figure 1: Simulation of a Typical Temperature Distribution Generated by a Gravity Wave between 86 km and 104 km**

One option to derive the temperature field in the upper atmosphere is to measure the oxygen A-band emissions near 762 nm. The long radiative lifetime assures that the molecules are in rotational equilibrium with the ambient atmosphere<sup>8</sup>.

The vertical distribution of O<sub>2</sub> A-band emissions as shown in Fig. 2 can be observed from 150 km down to about 60 km where the lines become optically thick. The different chemical processes are illustrated in the figure with the Barth process being the only one active at night.

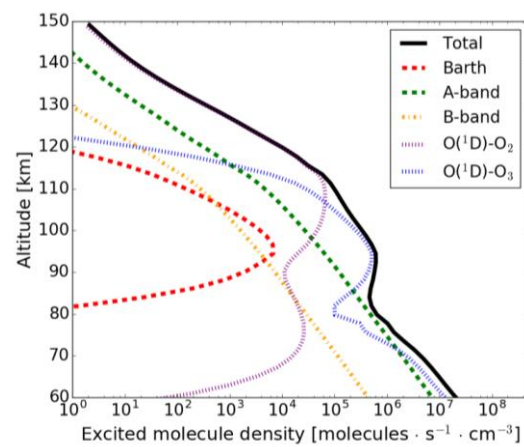


**Figure 2: Vertical Distribution of oxygen A-band emissions**

Figure 3 gives the spectral distribution of the emission lines with selected lines marked in different colors. The line intensities are calculated based on equations given by Song et al.<sup>9</sup>. Since the rotational structure of the O<sub>2</sub> A-band depends on the temperature following Boltzmann's law, the ratio of different rotational lines allows for temperature retrieval. The temperature dependence of selected lines are illustrated in the small insertion of the figure.

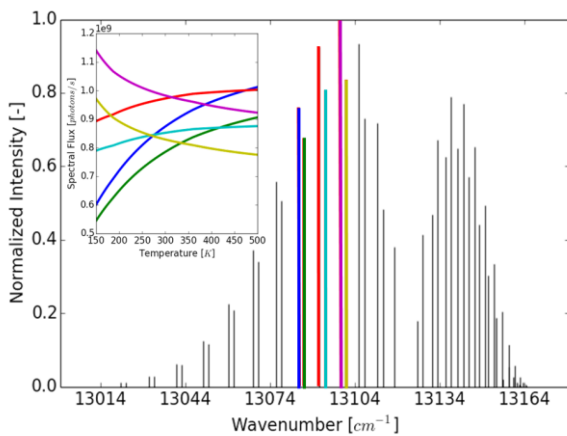


**Figure 3: Temperature Dependence of O<sub>2</sub> A-band**

Since relative intensities are measured only, there is no need for a precise absolute radiometric calibration of the instrument. Another advantage of measuring these emission lines is that the oxygen A-band emits at wavelengths below 1  $\mu\text{m}$ . So silicon based optical sensors operating at ambient or moderately cooled conditions can be used for signal detection. This reduces power consumption, mass, and costs of such an instrument significantly<sup>10</sup>.

### A SPATIAL HETERODYNE INTERFEROMETER FOR REMOTE SENSING

For the study of faint light signals from the atmosphere, interferometers have major advantages over conventional grating spectrometers. Their throughput is typically more than two orders of magnitude larger than for grating spectrometers of the same size. A Spatial Heterodyne Interferometer (SHI) is based on a concept originally proposed by Pierre Connes<sup>11</sup> in 1958, but the technology in those days was inadequate to build reasonable instruments. Recent developments in imaging technology and optical materials allow for useful applications of spatial heterodyne interferometry. An SHI is similar to a Michelson interferometer, where the mirrors are replaced by tilted diffraction gratings as illustrated in Fig. 4. Since a Spatial Heterodyne Interferometer (SHI) can be designed with no moving

parts, it can be built as a monolithic block which makes it very attractive for remote sensing, especially from space. Combined with a two-dimensional imaging detector, it records multiple interferograms of a scene, while one dimension provides the spectral information and the spatial information is found in the second dimension.

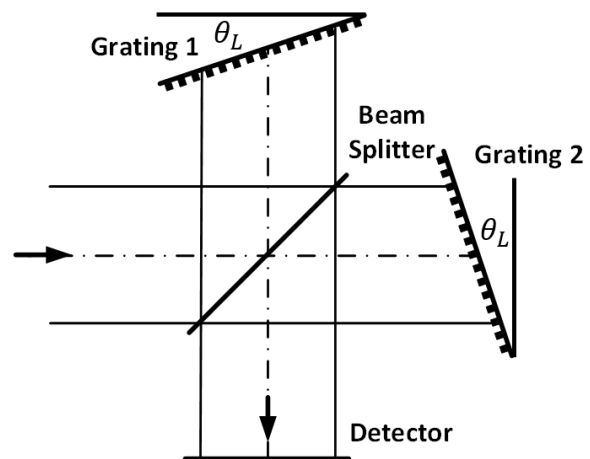


**Figure 4: Schematic of an SHI**

Due to the dispersion of the gratings, diffracted light waves show a wavefront tilt depending on the wavelength. This tilt leads to interference fringes in the detector plane with a characteristic spatial frequency for each incoming wavelength. The resulting interference pattern is the incoherent superposition of these patterns and can be analyzed by applying a numerical Fourier transform. Thus, the original wave spectrum can be determined. An SHI can be designed to resolve individual emission or absorption lines, while the optical throughput is still high.

The tilt angle of the gratings with respect to the incoming wave front is called Littrow angle  $\Theta_L$ , which is the key design parameter of an SHI (see Fig. 4). Light at the Littrow wavelength is returned in the same direction as the incoming path, resulting in an interference pattern with no spatial structure. Waves with wavelengths deviating from the Littrow wavelength are diffracted back from the gratings at a slightly different angle, introducing a wavelength dependent tilt which encodes the spectral information. The spatial frequency seen at the detector depends on the difference between the emission wavelength and the Littrow wavelength.

The acceptance angle of an SHI can be increased significantly, if prisms are inserted into the two

interferometer arms<sup>12</sup>. Depending on the actual design, the prisms increase the throughput of an SHI by 1–2 orders of magnitude. Figure 5 illustrates the SHI design (a) and provides an image of the prototype (b). With dimensions of 38 mm x 38 mm x 27 mm, it fits well into a CubeSat<sup>13</sup>.

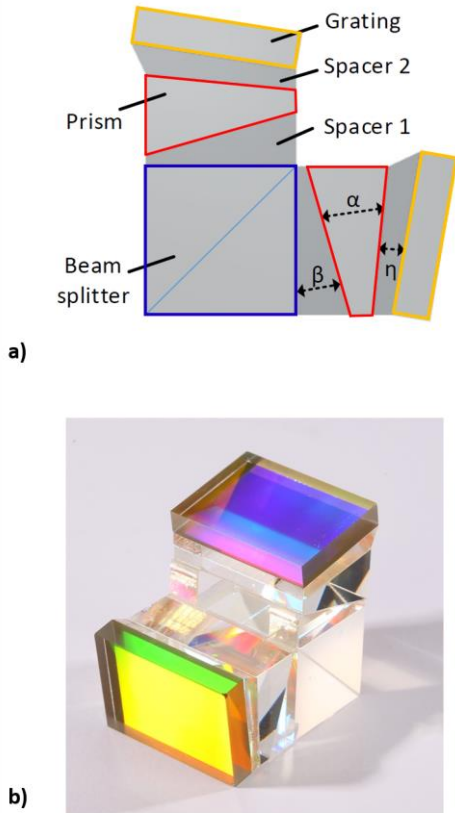


Figure 5: SHI: (a) design and (b) prototype

In order to determine the expected signal-to-noise ratio of the instrument for a given integration time, the amount of incoming light, which is available in the modulated part of the interferogram, and the noise of the detector has been calculated. In an SHI, 50% of the incoming radiation is lost at the beam splitter. Due to the fact that typical gratings have an efficiency of about 70% at 765 nm, another 30% of the radiation is not available. The contrast of the interferogram is further reduced by misalignments and aberrations of optical components, so that about 10-30% of the atmospheric signal can be expected in the modulated part of the interferogram. The simulated detector image of the O<sub>2</sub> A-band nighttime emission in a focused configuration is shown in Fig. 6, while the spectrum of an idealized Fourier-transformed interferogram is given in Fig. 7.

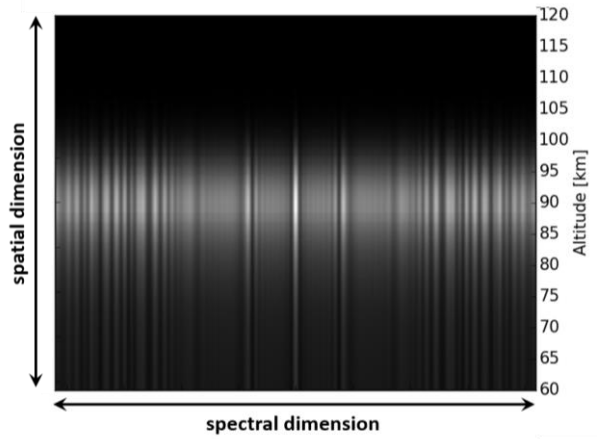


Figure 6: Simulated SHI Image of the O<sub>2</sub> A-Band Nighttime Emission

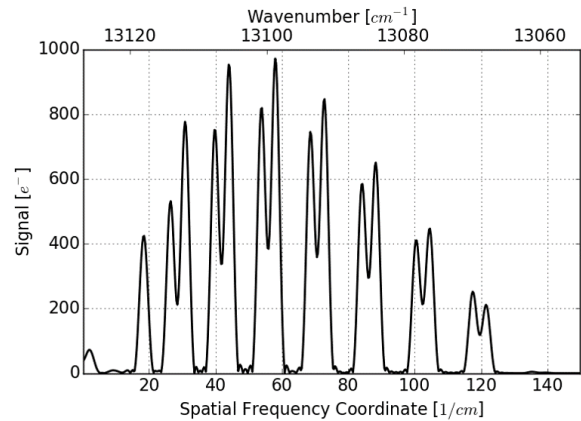


Figure 7: Spectrum of an Idealized Fourier-transformed Interferogram

## ATMOCUBE A1 LIMB SOUNDER

### Optical Design

In order to measure vertically resolved interferograms, a front optics is needed for imaging the atmospheric scene onto the gratings. A large aperture with a diameter of 75 mm leads to a high etendue (throughput) of 0.02 cm<sup>2</sup>sr, while a bandpass filter selects a narrow wavelength range (3.4 nm) in order to avoid adverse photons in the optical system. The optical design of the AtmoCube A1 prototype is illustrated in Fig. 8. The detector optics images the illuminated area of the gratings onto the Limb Sounding Detector (LSD), creating a set of interferograms. An additional stray light baffle in front of the system shall protect the

instrument from inadvertent radiation reaching the detector.

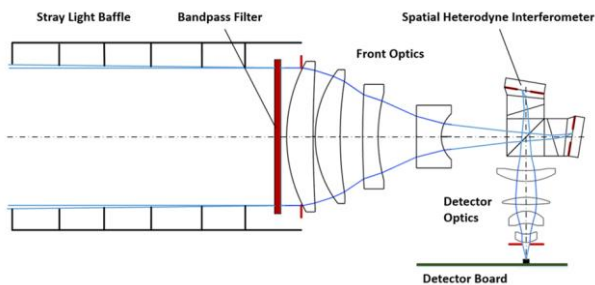


**Figure 8: AtmoCube A1 prototype optical design**

Depending on the launch opportunities, a wide range of orbit altitudes are acceptable. The front optics has a field of view of 1.3 deg, which corresponds to a vertical range of 50 to 80 km at the Earth limb with orbit altitudes between 400 and 1000 km. Assuming an orbit altitude of 600 km, the front optics is designed in such a way that an area of 60 km x 60 km at the limb in the range of 80 to 140 km can be observed (see Fig. 9). Spatial binning is variable and depends on emission intensity and integration time. A single detector pixel sees an atmospheric element of approximately 200 m in the vertical. The envisaged attitude resolution is 1.5 km. Since the distance between the satellite and the tangent point is between 2,300 and 3,500 km, a highly precise attitude control in the sub-arcmin range is required.

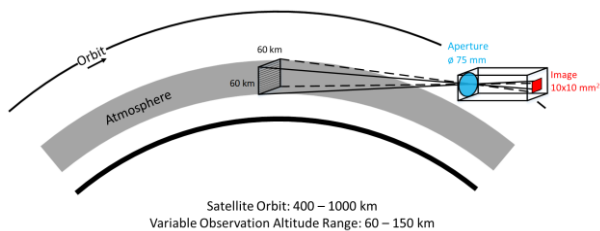


**Figure 9: Limb view of the AtmoCube A1 satellite**

### ***Thermally controlled image sensor***

Since the airglow is a faint phenomenon, high quality imaging under extremely low light is mandatory. A back-side illuminated scientific CMOS image sensor 4.2 Megapixel resolution is used. The large optical area (22.5mm x 22.5mm) matches well with the image size of the atmospheric scene on the gratings. The sensor has an extremely low readout noise of 1.6 e- and a high quantum efficiency of about 70% at 760 nm. The integration time will be up to several seconds

depending on the atmospheric conditions (daytime or nighttime).

The detector shall be operated at a temperature between -30°C and 0°C in order to increase the signal-to-noise ratio. To maintain the temperature in this range during operation, a Thermal Control Unit (TCU) is needed. A passive radiator facing deep space will be installed on one side of AtmoCube A1. Power consumption of the detector unit is about 2 W. To radiate the dissipated heat into space a black coated radiator surface of 120 mm x 120 mm is sufficient.

### ***Payload Electronics***

The AtmoCube A1 payload electronics controls two imagers, the Limb Sounding Detector (LSD) of the instrument and the additional Albedo Cloud Detector (ACD). It consists of two functional blocks, the proximity electronics (PXE) for directly interfacing to several detector ICs and the frontend electronics (FEE) with an embedded controller, which serves as the central processing system. The FEE handles signals from the CubeSat bus to start the measurement, to acquire detector data, to provide data pre-processing (e.g. data binning) and to transfer data to the command and data handling (C&DH) subsystem.

The electronics design uses state of the art, commercial-of-the-shelf (COTS) components with an adapted approach to achieve radiation tolerant characteristics considering adequate mitigation techniques. The electronics combines hardware and software redundancies to improve system availability and reliability for long life missions.

The system controller of the FEE is based on a System-on-Chip (SoC) architecture, which combines reconfigurable logic with a dual core processor system. The system controller boots from an on-module flash memory or a solid state disc device which provides a reference boot image in redundancy. The operation of the system controller is checked by a watchdog timer (WDT), which triggers a reset signal in case of a firmware violation or logic malfunction. Processor memory failures are mitigated by using memory chips with integrated error code correction, periodic memory pattern and cycling redundancy checks on selected data structures. The logic configuration is placed in triple-module-redundancy and the majority voters generates an index signal in case of a discrepancy.

The image sensors, PXE and FEE are protected against single event latch up (SEL) using overcurrent protection circuits. The payload electronics can operate from common CubeSat bus voltages and generate the internal

supplies with redundant Point-of-Load (POL) converters.

The communication is divided into two channels: The telecommand interface which controls the instrument and acquire housekeeping values and the science data interface which sends the detector data to the C&DH. Each channel is implemented as a redundant logic core and can be a combination of different physical interfaces in case of limited resources.

### ATMOCUBE A1 DESIGN

The AtmoCube A1 limb sounder consists of the optics, the electronics and the thermal control unit as described in the previous chapter. The mass of the payload is less than 3 kg with a power consumption of less than 8 W. The data rate can be reduced to 300 kbit/s by pixel binning. Since limb viewing measurements require highly precise attitude control and determination, attitude control accuracy in pitch shall be about 0.003 deg, which corresponds to an uncertainty in altitude determination of 140 m from a 600 km orbit. Detailed payload specifications are given in Table 1.

The AtmoCube A1 payload is designed for a six unit (6U) CubeSat. Besides the main payload, an Albedo Cloud Camera (ACC) for the detection of stray light reflected from tropospheric clouds is included in the AtmoCube concept. As in all CubeSat systems, solar panels, an electrical power system, an attitude determination and control system (ADCS), an onboard computer, and an S-band antenna for communication is needed. As shown in Fig. 10, all these components are compiled to fit into a 6U CubeSat.

**Table 1: AtmoCube A1 Limb Sounder specifications**

Optics	
Aperture	Ø 75 mm
Etendue (Throughput)	0.02 cm <sup>2</sup> sr
Atmospheric limb image	60 km x 60 km
Variable altitude range	60 km – 150 km
Altitude resolution	< 1.5 km
Spectral range	761 – 765 nm
Max. resolving power ( $\lambda/\Delta\lambda$ )	18 500
Detector	
image sensor	CMOS
Number of pixels	2048 x 2048
Quantum efficiency	0.7 at 760 nm
Thermal control	deep space radiator
Instrument	
Mass	< 3 kg
Volume	~ 4 liters
Power	< 8 W
Data rate after binning	300 kbit/s
Attitude control accuracy	0.003 deg (pitch)
Operating temperature	-40°C to 50°C

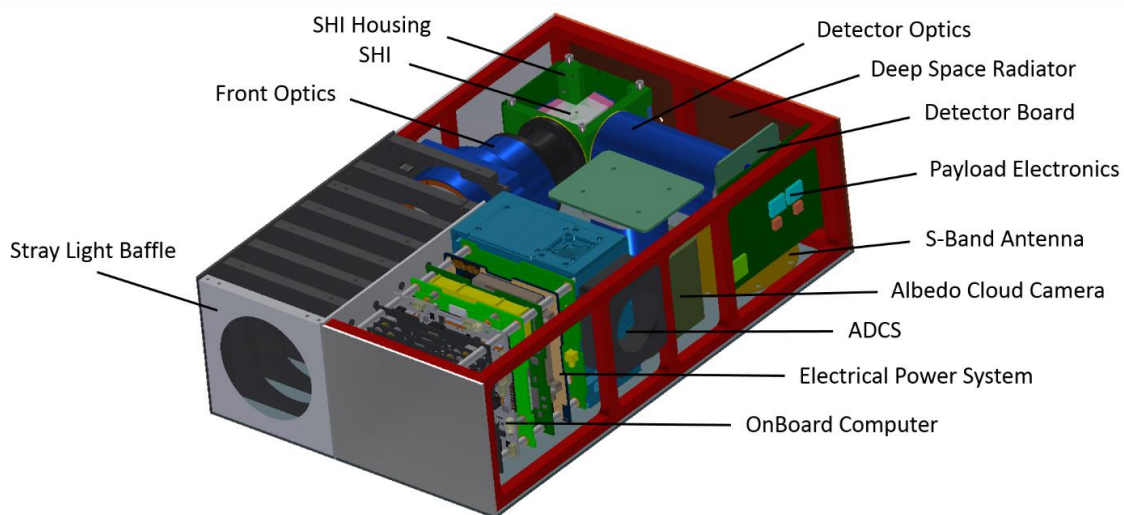


**Figure 10: AtmoCube A1 satellite design**

## ATMOCUBE A1 OPERATIONAL MODES

The agility of a CubeSat shall be used to focus the measurements on specific regions from different viewing angles. In order to measure gravity waves at high spatial resolution making multi-angle observations, CubeSat agility can be used by sweeping the line-of-sight through specific regions of interest to derive a three-dimensional image of an atmospheric volume using tomographic reconstruction techniques. Typical slew rates for a 6U CubeSat of 5 - 10 deg/sec can be achieved by the ADCS. Two potential observation modes for a single spacecraft mission are illustrated in Fig. 11. For illustration purposes, an image of the Moderate Resolution Imaging Spectroradiometer (MODIS) on NASA's Terra satellite is used as background, where a large-scale, overlapping wave pattern in the sun glint region of the Arabian Sea was captured. The red inverted triangles mark the tangent points of the limb measurements. An integration time of 10 seconds and a slew rate of 5 deg/sec correspond to a sampling rate of 100 km at the tangent point.

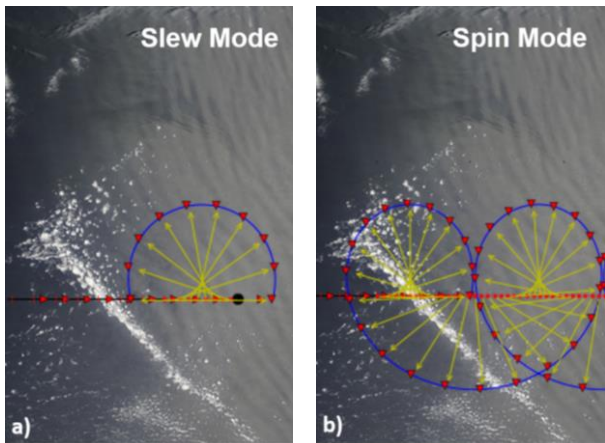


Figure 11: AtmoCube A1 operational modes

The final goal is a constellation of several satellites that view a region of interest from different perspectives<sup>14</sup>. An artist's concept of an AtmoCube constellation is given in Fig. 12. Details on the optimal satellite constellation will follow at a later stage. Final constellation also depends on the number of satellites, their maneuverability and other factors.

## PAYLOAD IN-ORBIT VERIFICATION TEST

On December 22, 2018 the first version of the instrument named AtmoSHINE (Atmospheric Spatial Heterodyne Interferometer Next Exploration) was launched onboard a Chinese in-orbit demonstration satellite. From a near-Earth dust-dawn orbit of 1100 km

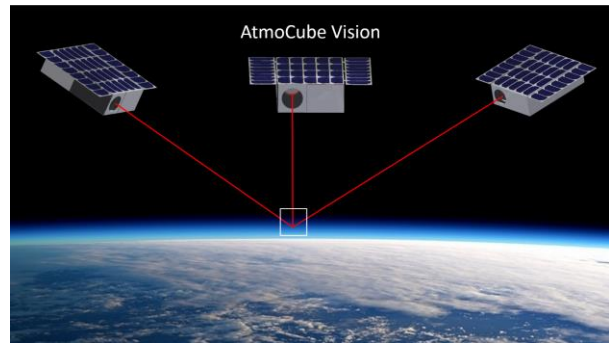


Figure 12: Artist's concept of an AtmoCube constellation

altitude, AtmoSHINE measures the global distribution of the O<sub>2</sub> A-band nightglow emissions. Figure 13 shows the fully tested AtmoSHINE Flight Model which was delivered only ten months after project start.

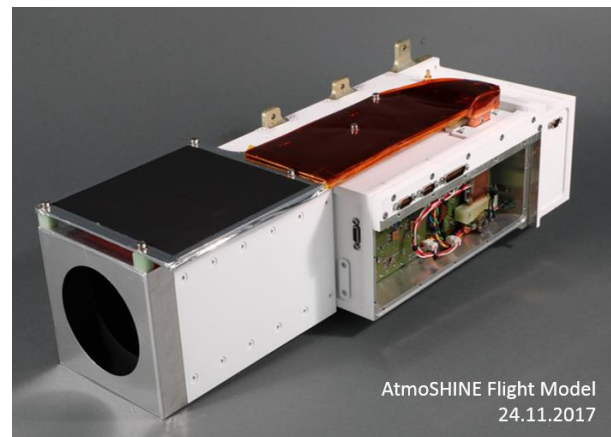


Figure 13: AtmoSHINE Flight Model

## SUMMARY AND OUTLOOK

As the features of the MLT region are valuable proxies of climate change, advanced measurement techniques are needed in order to provide detailed information about the dynamical disposition of the upper atmosphere. To measure three-dimensional gravity wave fields at those altitudes is still a challenge for satellite instruments. A spatial heterodyne interferometer has been developed to measure oxygen A-band emissions between 60 and 120 km altitude globally. As an SHI has no moving parts, it can be built as a monolithic block, which makes it very attractive for atmospheric measurements, especially from space. It fits into a small volume and still has an excellent throughput along with high spectral resolution. Interferograms from different altitudes can be measured simultaneously. The agility of a CubeSat shall be used

to detect dynamical structures in the MLT region by a tomographic approach. The final goal is a constellation of several satellites that view a region of interest from different perspectives.

### References

1. Beig, G., “Long-term trends in the temperature of the mesosphere/lower thermosphere region”, *J. Geophys. Res.*, 116, A00H11, 2011.
2. Vincent, R.A., “The dynamics of the mesosphere and lower thermosphere: a brief review”, *Prog. in Earth and Planet. Sci.*, 2015.
3. Shepherd, T.G., “Atmospheric circulation as a source of uncertainty in climate change projections”, *Nature Geoscience*, Vol. 7, 703-708, 2014.
4. Smith, A. K., Pedatella, N. M., Marsh, D. R., & Matsuo, T., “On the dynamical control of the mesosphere-lower thermosphere by the lower and middle atmosphere”, *Journal of the Atmospheric Sciences*, 74, 933–947, 2017.
5. Kim, Y.-J., Eckermann, S.D., and Chun, H.-Y., “An overview of the past, present and future of gravity-wave drag parametrization for numerical climate and weather prediction models”, *Atmosphere-Ocean*, Vol. 41, 65-98, 2003.
6. Baumgarten, G., & Fritts, D. C., “Quantifying Kelvin-Helmholtz instability dynamics observed in noctilucent clouds: 1. Methods and observations”. *Journal of Geophysical Research: Atmospheres*, 119, 9324-9337, 2014.
7. Ward, W. E.: A simple model of diurnal variations in the mesospheric oxygen nightglow, *Geophys. Res. Lett.*, 26, 3565–3568, 1999.
8. Lübken, F.-J., Berger, U., & Baumgarten, G., “On the anthropogenic impact on long-term evolution of noctilucent clouds”. *Geophysical Research Letters*, 45, 6681–6689, 2018.
9. Song, R., Kaufmann, M., Ern, M., Ungermann, J., Liu, G., and Riese, M., “Three-dimensional tomographic reconstruction of atmospheric gravity waves in the mesosphere and lower thermosphere (MLT)”, *Atmos. Meas. Tech.*, 11, 3161-3175, 2018.
10. Kaufmann, M., Olschewski, F., Mantel, K., Solheim, B., Shepherd, G., Deiml, M., Liu, J., Song, R., Chen, Q., Wroblowski, O., Wei, D., Zhu, Y., Wagner, F., Loosen, F., Froehlich, D., Neubert, T., Rongen, H., Knieling, P., Toumpas, P., Shan, J., Tang, G., Koppmann, R., and Riese, M., “A highly miniaturized satellite payload based on a spatial heterodyne spectrometer for atmospheric temperature measurements in the mesosphere and lower thermosphere”, *Atmos. Meas. Tech.*, 11, 3861-3870, 2018.
11. Connes, P., “Spectromètre interférentiel à sélection par l'amplitude de modulation”, *J. Phys. Radium*, Vol. 19, 215-222, 1958.
12. Hilliard, R. L. & Shepherd, G., “Wide-Angle Michelson Interferometer for Measuring Doppler Line Widths”, *Journal of the Optical Society of America*, Vol. 56, 362-369, 1966.
13. Deiml, M., “Development of a Small Satellite Remote Sensing Payload for Passive Limb Sounding of the Atmospheric Oxygen Emission”, PhD thesis, Univ. Wuppertal, 2017.
14. Olschewski, F., Kaufmann, M., Mantel, K., Riese, M., Koppmann, R., “A novel CubeSat payload for airglow measurements in the mesosphere and lower thermosphere “, *Proc. SPIE 10769, CubeSats and NanoSats for Remote Sensing II*, 1076903, 2018.